Anomaly Detection in Gamma-ray Radiation Spectra using Artificial Neural Network and Ant Colony Optimization

Assem Abdelhakim

Department of Radiation Engineering, National Center for Radiation Research and Technology (NCRRT), Egyptian Atomic Energy Authority, Cairo, Egypt.
E-mail addresses: assem.abdelhakim@eaea.org.eg

Abstract: Detection of threatening radioactive sources is a crucial task for homeland security. One of the major challenges in radiation detection is to distinguish between the background radiation and the anomalous source radiation from the measured radiation spectrum at low source to background ratio. In this paper, an anomaly detection technique is proposed to detect anomalous Gamma-ray radiation spectra using machine learning. The method is based on dividing the radiation spectrum into two sub-spectra, where the background part of the second sub-spectrum is predicted from the first sub-spectrum through a neural network model. Hence, an anomaly spectrum is detected according to the difference between the predicted background radiation data and the measured values of the second sub-spectrum. The ant colony optimization is utilized to select, from the radiation spectrum, the values assigned to the first and second sub-spectra, where optimum prediction accuracy can be provided. To present the effectiveness of the proposed work, a performance comparison is conducted with both benchmark and a recent neural network-based method. The performance is evaluated using real data that represent both background and radioactive source radiation, which are measured through a network of detectors. Experimental results show that the proposed method outperforms the other methods in terms of the detection capability even at low source to background radiation ratios.

Keywords: Anomaly detection; Machine learning; Neural Network; Ant colony optimization; Gamma-ray radiation spectrum.

1 Introduction

Radioactive sources are widely used for many purposes such as industrial, medical, agricultural, and research. However, due to the dangerous effect of radiation on public safety, lost or stolen sources can present a major threat. Many radiation source incidents have occurred in many countries according to the international atomic energy agency (IAEA) records [1]. Hence, radiation anomaly detection is considered to be a crucial task for homeland security, where anomalous nuclear sources can be detected based on the data provided by radiation detectors.

Anomaly detection is generally used to find the observation data instances that deviate from normal (typical) date. In radiation detection, normal data represent the background radiation. On the other hand, anomaly data represent additional

anomalous source radiation to the background radiation. Detecting anomalous sources at low source to background ratios has been always a challenging task, where the detected anomalous source radiation is weak compared to the background radiation. Significant research efforts have been carried out for developing detection algorithms that can enhance the detection accuracy.

Many radiation anomaly detection methods have been proposed. In [2], a detection algorithm based on energy windowing was presented, where the ratio between the radiation data at low and high energies was used to discriminate between background and anomalous radiation. Various energy windowing methods were implemented, in [3], to study their performance for radiation portal monitoring, which is employed to check cargos at international border crossing. Energy windowing methods are mainly designed for detecting radioactive materials with large count rates, which are considered as threatening sources. However, at low source to background radiation ratios, the energy windowing technique will not provide an effective detection capability.

In [4,5], the spectral comparison ratios (SCR) method was studied, where the ratios between the data of the first radiation spectral bin and that of the other bins are used for anomaly detection. The method is based on comparing the count ratios of a given radiation data with that of the background data predicted using Kalman filter at the time of detection. Certain radiation sources are considered by injecting simulated values into the background data. Results showed that the SCR method can achieve good detection sensitivity to targeted sources. However, the sensitivity of the method came at the price of generality.

One of the commonly used approaches for radiation anomaly detection is the principal component analysis (PCA) [6-9]. Mostly, PCA is applied for dimensionality reduction by projecting the data onto a lower dimensional space. In [6], an analysis was carried out to investigate each principle component as an anomaly score for two radiation sources. Results showed that the first few principle components present better anomaly scores than the other components. Another method in [9] was proposed to detect anomalous data by evaluating the Mahalanobis distance between the principle components of a given radiation data and that of the normal observations. The classification performance of the method depends dramatically on the radiation source data.

To further improve the anomaly detection performance, machine learning models are employed. Generally, anomaly detection techniques that are based on machine learning can be categorized into supervised, unsupervised, and semi-supervised according to the available labels of the training data. For radiation anomaly detection, semi-supervised learning is usually applied, where only the labeled normal data instances are available for training. However, most of the recent radiation anomaly detection methods are based on neural network [10-18] due to its significant classification performance, which requires supervised learning using labeled data.

Accordingly, neural network-based methods are usually employed for detecting and identifying certain radiation sources.

In [17], a multiphase neural network was trained, where each phase divides the input data according to a given metric until a high accurate classification was achieved in the last phase. In [18], a fully-connected and convolutional neural network models were combined for radiation source detection. Some feature values, like peak-ratios, discrete cosine transform coefficients, and spectrum counts were extracted from the radiation data through which the hybrid model can perform the classification. The method outperforms other neural network-based methods in terms of detection accuracy. However, the training of the hybrid model is more time consuming than that of the other neural network models.

Practically, designing a generic radiation anomaly detection method is carried out using only the background radiation data, where any anomalous source can be detected. Hence, conventional neural network-based methods may not be suitable for non-specific anomalous radiation source detection. Recently, autoencoders have been used for detecting any anomalous radiation data, which are based on a neural network structure. Autoencoders are mostly used for compression or dimensionality reduction. Accordingly, in [14], an autoencoder was trained using only the background data to detect anomalous radiation based on the reconstruction error between the output and the input of the autoencoder.

To the best of our knowledge, most of the recent methods can be categorized as classifier-based detection techniques, where supervised learning is required using anomalous measurements corresponding to certain sources. According to the studies in the literature, classifier-based detection methods can perform high classification accuracy. However, there are some general disadvantages of classifier-based anomaly detection methods. Practically, the anomaly data samples are not commonly available for training the classifier model. Also, after training the classifier model, the detector cannot be tuned for adjusting the detection sensitivity to encounter environmental changes that may impact the false alarm rate. Furthermore, the receiver operating characteristics (ROC) cannot be computed for performance evaluation, which is a significant metric used to visualize the tradeoffs between true alarm rates and false alarm rates [13].

In this work, a threshold-based radiation anomaly detection method is proposed using the neural network as a regression model to achieve high accuracy, where only the background data are used for training. The anomaly detection is performed according to a numerical anomaly score value and a user-defined threshold value. Hence, the detection sensitivity can be easily adjusted by modifying the threshold value. In the following, the contribution of the work is summarized:

1- Employing neural network regression model to detect anomalies in radiation data using only the normal data for model training.

2- Implementing a method for simulating anomalous data from the normal data to consider different anomalies in the model training.
3- Applying ant colony optimization to select the best values for the parameters of the proposed method.
4- Designing a fitness function for the optimization process through which an optimum detection performance can be provided.
5- Using real (normal and anomalous) radiation data, measured by a network of detectors, for evaluating the proposed method using the receiver operating characteristics curve.

The rest of the paper is organized as follows: Section 2 presents a briefly introduction to the ant colony optimization. In Section 3, the proposed work is explained. The experimental results are illustrated in Section 4. Finally, the work is concluded in Section 5.

2 Ant colony optimization

The Ant Colony Optimization (ACO) is mainly used for solving discrete optimization problems. It was first presented by Colorni et.al [19], which simulates the ants behavior for selecting the shortest path to the food source. Initially, ants explore randomly different paths, where each ant deposits on its path to the food source a substance referred to as pheromone. When more ants walk on the same path, the pheromone concentration on that path increases. Usually, the path with the highest pheromone concentration represents the shortest path to the food source. Accordingly, ants select the paths that have the highest pheromone concentration to reach the food source quickly.

For any meta-heuristic optimization method, such as the ACO algorithm, a solution space (S) and a fitness function (F) must be defined. Then the optimization algorithm can be applied to find the solution S_{opt} that optimizes (maximizes or minimizes) the fitness function F. The objective of a discrete optimization problem is to select the best decision value for each of the considered D variables, where D is the dimension of the solution space. In the ACO algorithm, the solution space represents the area between the nest and the food source, which is divided into regions that represent the solution variables. For each region, there are a limited number of paths that are represented by the corresponding decision values. Fig. 1 shows an example for a 4-dimensional solution space $S = [s_1, s_2, s_3, s_4]$, where the variables s_1, s_2, s_3, and s_4 have 6, 4, 5, and 3 decision values, respectively. The path selected by the k^{th} ant represents the k^{th} solution $S_k = [s_{14}, s_{22}, s_{31}, s_{42}]$ as shown from Fig. 1.

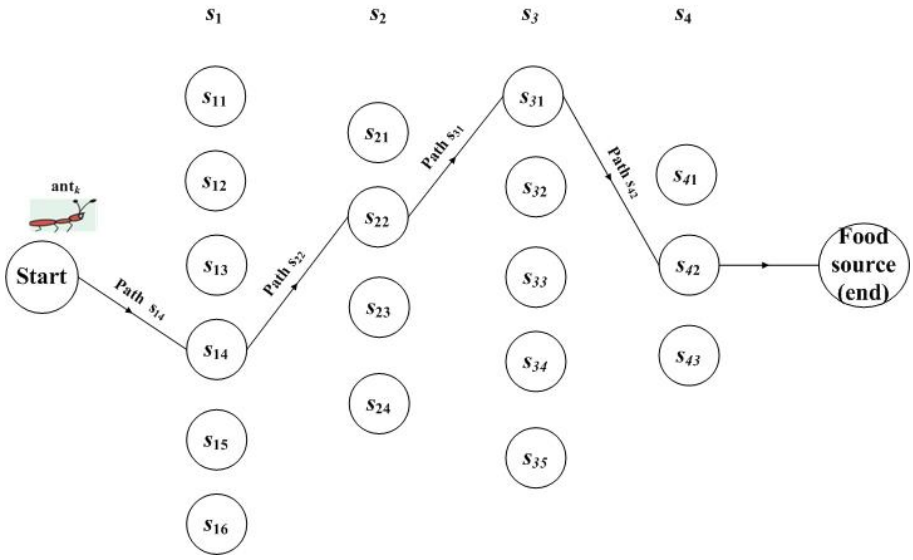

Fig. 1 A path (solution) selected by the k^{th} ant, from a 4-dimensional solution space, where s_{14}, s_{22}, s_{31}, and s_{42} represents the decision values of the k^{th} solution.

ACO is a population-based optimization method that operates in an iterative manner, where a number of solutions are explored per iteration. Fig. 2 shows the procedure for selecting the optimum solution using ACO optimization. The parameters to be defined are the number of solutions to be explored per iteration, initial pheromone concentration, and the number of iterations N_{itr}. Initially, all solutions are assigned the same initial pheromone level. Then a set of solutions are selected randomly. The fitness function is used to evaluate the fitness value for each solution. According to the fitness value, the pheromone concentration for each explored solution (path) is updated [20]. Higher pheromone concentration is assigned to solutions with better fitness values. A new set of solutions are selected, to be explored, based on the new pheromone concentration levels. The process is repeated for a number of iteration N_{itr}. Finally, the solution with the best fitness value is selected to represent the optimum solution. More details about the ACO algorithm can be found in [19-23].

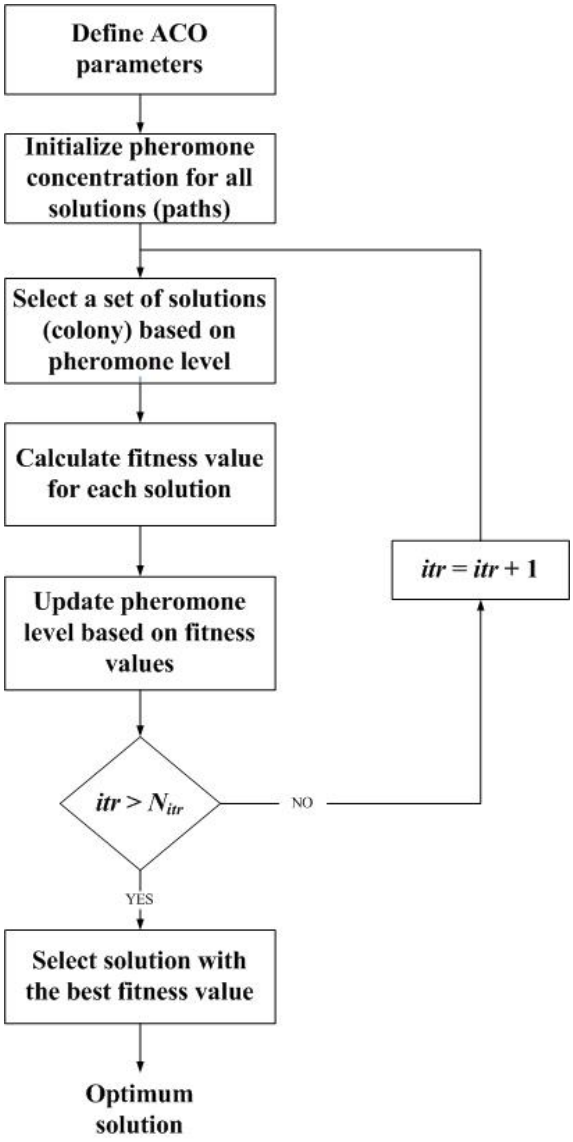

Fig. 2 The procedure for selecting the best solution using ACO optimization

3 The proposed work

3.1 Neural Network-based radiation anomaly detection

In this sub-section, the proposed radiation anomaly detection method is described in details. The method is based on the relation between the counts of the detected radiation spectrum *RS* that can be represented as follows:

$$RS = \begin{bmatrix} C_1 \\ C_2 \\ \vdots \\ C_{N_b} \end{bmatrix}, \quad (1)$$

where C_i is the radiation count measured at the i^{th} spectral bin, while N_b is the total number of bins. The given radiation spectrum RS is divided into two sub-spectra denoted by RS_1 and RS_2. In the proposed work, Set_1 and Set_2 represent two sets that include the bin numbers of the spectrum RS, where the count values of RS_1 and RS_2 are selected, respectively, as follows:

$$RS_1[i] = RS[Set_1[i]],\ RS_2[j] = RS[Set_2[j]],\ i = 1, 2, \cdots, N_1,\ j = 1, 2, \cdots, N_2, \quad (2)$$

where N_1 and N_2 are the total number of spectral bins selected for RS_1 and RS_2, respectively. Then a neural network model is used to predict the background counts of RS_2 from the counts of RS_1. The anomaly detection can be performed according to the difference between the measured RS_2 and the predicted background counts. Note that RS_1 and RS_2 can be represented by the summation of the background and the anomaly source counts as follows:

$$RS_1 = B\_RS_1 + S\_RS_1,\quad RS_2 = B\_RS_2 + S\_RS_2, \quad (3)$$

where B_RS_1 and B_RS_2 are the vectors of count values representing the background radiation from the respective RS_1 and RS_2 sub-spectra. On the other hand, S_RS_1 and S_RS_2 are the vectors of count values representing the anomaly source radiation from RS_1 and RS_2 sub-spectra, respectively. For a background radiation spectrum, the count values of S_RS_1 and S_RS_2 should be equal to zero. Hence, for anomaly spectra, the difference between the measured RS_2 and the predicted B_RS_2 is expected to be larger than that for the background spectra.

Training the neural network model is performed using the background spectra. Hence, the model's output B_RS_2 is equal to RS_2. A feature vector is used to represent the model's input that includes the sub-spectrum RS_1. To provide effective prediction, the average count value of the radiation spectrum is used as a feature value along with the RS_1 counts as follows:

$$fv = \begin{bmatrix} C_{avg} \\ r_1 \\ r_2 \\ \vdots \\ r_{N_1} \end{bmatrix}, \quad (4)$$

where C_{avg} is the average count value of the given RS spectrum, while r_i is the i^{th} count value of the RS_1 sub-spectrum. Fig. 3 shows the feature extraction process, where the feature vector is calculated from the given radiation spectrum.

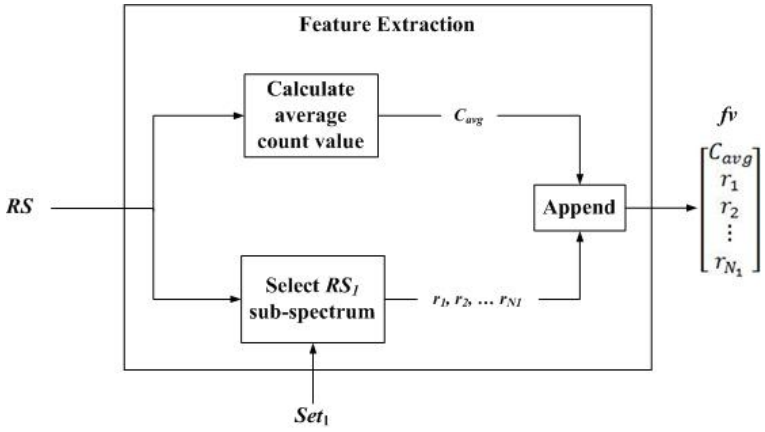

Fig. 3 The feature extraction process of the proposed work

To consider both normal and anomaly spectra in the model training, a function is used for generating (simulating) anomaly data from the background spectra. Algorithm 1 shows the pseudo code for generating an anomaly spectrum from a given normal spectrum. The algorithm is used to modify only the RS_1 sub-spectrum of the given RS spectrum. Accordingly, Set_1 must be provided to the function. It should be noted that two conditions are applied to consider anomaly data from a radiation source, which are: 1) Anomaly counts are greater than the background counts, i.e. values can only be increased. 2) Not all bin values are modified at the same time because each radiation source affects count values at certain energy levels. Hence, a number of N_p counts are selected to be modified, where N_p is calculated using the *rand_int*(., .) function that generates a random integer between a given minimum and maximum values. As shown from Algorithm 1, the minimum and maximum values of N_p are 2 and $N_1/2$, respectively. Moreover, the indices of the N_p count values are selected randomly from the range [1: N_1] using the function *Random_selection*(N_1, N_p).

Algorithm 1. *Generate_Anomaly*

Inputs:

- Normal data vector: R
- Set of bin numbers: Set

Begin

1. $R_a = R$ //Initialization
2. $N_1 = ||set||$ // ||.|| returns the number of values in a given list
3. N_p = *Rand_int*(2, $N_1/2$)
4. *Index_sel* = *Random_Selection* (N_1, N_p)
5. **For** i =1: || *Index_sel* ||
6. ind_i = *Index_sel* [i]
7. $R_a[set[ind_i]] = (1 + rand\ ) * R[set[ind_i]]$
8. **End For**

Output: The anomaly vector R_a.

In this work, N_D background radiation spectra are used for representing the normal dataset, which are divided into N_{tr} and N_{ts} spectra for training and testing the model, respectively, such that:

$$N_{tr} = \frac{8}{10} N_D \quad , \quad N_{ts} = \frac{2}{10} N_D \quad . \tag{5}$$

In Fig. 4, the training procedure for the NN model is presented using the N_{tr} background radiation spectra. The N_{tr} spectra are divided equally into two groups denoted by Group 1 and Group 2. As can be seen from Fig. 4, the spectra of the first group (Group 1) are used for generating the anomaly data through the *generate_anomaly* function. From each spectrum, the feature vector is calculated and the sub-spectrum RS_2 is selected. The neural network model is trained to predict the sub-spectrum RS_2 from the feature vector *fv* of the given spectrum *RS*. After training the model, the proposed radiation anomaly detection can be applied according to the block diagram presented in Fig. 5. The sub-spectrum S_RS_2, corresponding to the anomaly source, is calculated from RS_2 and the predicted B_RS_2 as follows:

$$S\_RS_2 = RS_2 - B\_RS_2 \quad . \tag{6}$$

According to the count values of S_RS_2, the spectrum *RS* can be classified as background or anomaly. Note that, for a background spectrum, the counts calculated for S_RS_2 should be equal to zero. However, the calculated counts may be greater than zero due to the prediction error of the neural network. Accordingly, for a given normal/anomaly radiation spectrum, the classification is carried out based on the Mahalanobis distance between S_RS_2 and the prediction error. First, the error is calculated for each radiation spectrum in the training background set to provide an error matrix E, of size $N_2 \times N_{tr}$, as follows:

$$E = \left[e_1 \; e_2 \cdots e_{N_{tr}} \right] \quad , \tag{7}$$

where e_i is the error vector, of length N_2, between the sub-spectrum RS_2 and the predicted B_RS_2 corresponding to the i^{th} background radiation spectrum. Then, for a given spectrum, the Mahalanobis distance is calculated between the corresponding sub-spectrum S_RS_2 and the error matrix E as follows:

$$d_M = \sqrt{S\_RS_2^T \bullet \Sigma^{-1} \bullet S\_RS_2} \quad , \tag{8}$$

where d_M is the Mahalanobis distance, while Σ is the covariance matrix of size $N_2 \times N_2$ calculated from the matrix of error vectors E. Finally, the anomaly detection is carried out by comparing the calculated Mahalanobis distance d_M with a user defined detection threshold, denoted by thr_d as shown from Fig. 4.

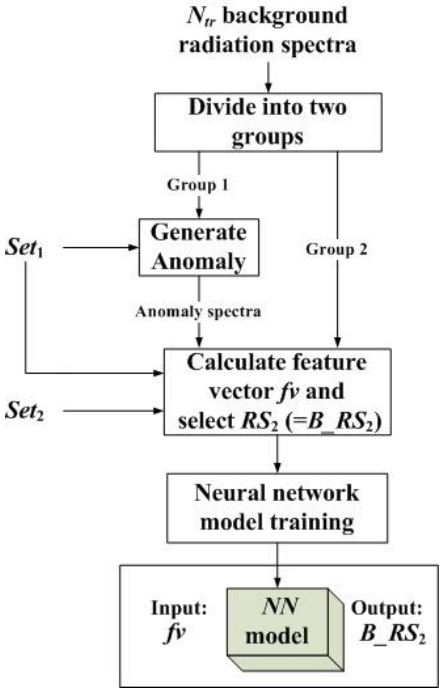

Fig. 4 Training the neural network model using N_{tr} background spectra

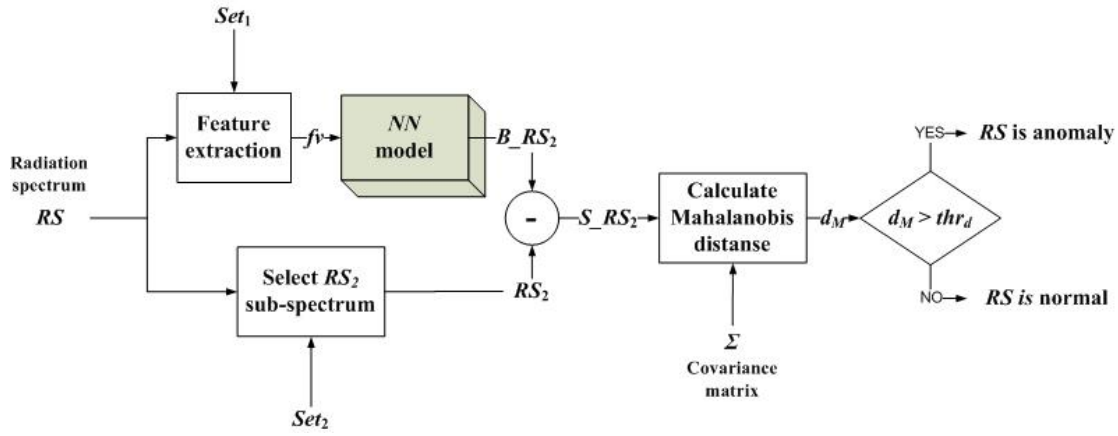

Fig. 5 The proposed radiation anomaly detection

3.2 Parameter optimization

In the proposed method, the selection of the spectral bins for Set_1 and Set_2 affects the detection performance. Hence, an optimization process is carried out before applying the proposed anomaly detection method to provide the optimum selection according to the detection accuracy. The ACO technique is employed to perform the required optimization. First, a fitness function is designed to represent the detection

performance as a function of the two sets (Set_1 and Set_2). Then, the ACO is used to select the optimum sets that maximize the designed fitness function.

For the considered optimization problem, the solution space is represented by all the feasible sets that can be selected for Set_1 and Set_2. Note that the spectral bin numbers in Set_1 and Set_2 are selected from the N_b bins of the given radiation spectrum, where the bin numbers included in Set_1 are not included in Set_2. Accordingly, the bin numbers assigned to Set_1 and Set_2 can be calculated from a vector V_b of N_b binary values represented as follows:

$$V_b = \begin{bmatrix} b_1 \\ b_2 \\ \vdots \\ b_{N_b} \end{bmatrix}, \quad (9)$$

Where the binary value of b_i indicates the assignment of the i^{th} spectral bin number to either Set_1 or Set_2 according to the following relation:

$$b_i = \begin{cases} 1, & assign\ the\ i^{th}\ bin\ to\ Set \\ 0, & assign\ the\ i^{th}\ bin\ to\ Set \end{cases} \quad (10)$$

To search for the optimum values of the vector V_b, the solution space must include all the feasible combinations that can be provided. Accordingly, the solution space may have a huge size for large values of N_b, which may decrease the convergence rate of the optimization process. Furthermore, Meta-heuristic optimization techniques are usually designed for multi-dimensional solution space. Hence, the vector V_b is divided into D sub-vectors of length L bits. Each sub-vector is converted to a decimal value to provide a D-dimensional vector X as follows:

$$X = \begin{bmatrix} x_1 \\ x_2 \\ \vdots \\ x_D \end{bmatrix}, \quad (11)$$

where x_i is the i^{th} decimal value calculated from V_b according to the following relation:

$$x_i = Bin2Dec\left(V_b[(i-1)\bullet L+1 \rightarrow i\bullet L]\right), \quad (12)$$

where *Bin2Dec*(.) is a function that converts a list of binary bits to the corresponding decimal value. Note that the number of bits L is equal to N_b/D. The solution space is defined by the range $[X_{min}, X_{max}]$ such that:

$$X_{min} = \begin{bmatrix} 1 \\ 1 \\ \vdots \\ 1 \end{bmatrix}, \quad X_{max} = \begin{bmatrix} 2^L - 2 \\ 2^L - 2 \\ \vdots \\ 2^L - 2 \end{bmatrix} \tag{13}$$

The minimum and maximum values of x_i are 1 and 2^L - 2, such that only the least significant bit of the corresponding binary values is equal to 1 and 0, respectively, as shown from Fig. 6. Thus, the minimum number of bins assigned to either Set_1 or Set_2 from each sub-vector of V_b is equal to 1.

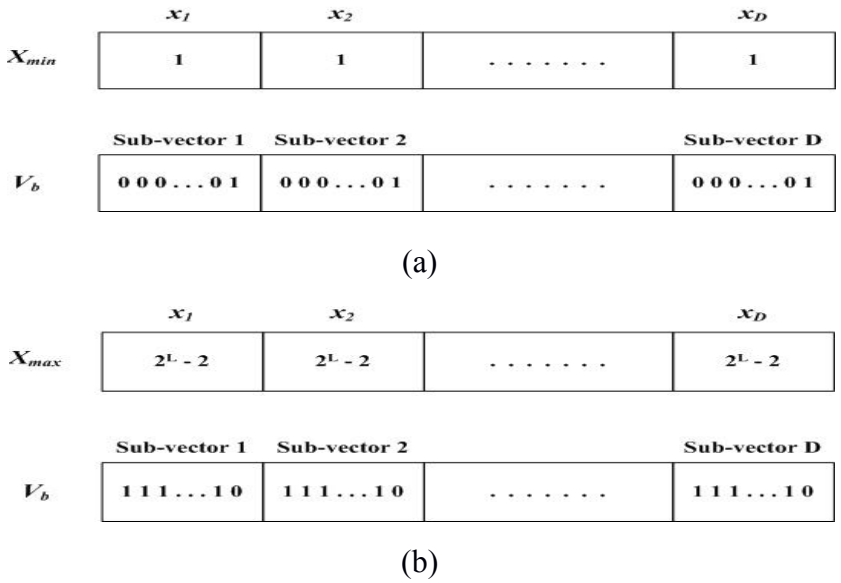

Fig. 6 The values of the solution vector X and the corresponding vector V_b for (a) X_{min}, and (b) X_{max}.

The evaluation of each selected solution X is performed through a fitness function. Fig. 7 shows the procedure of the designed fitness function. First, Set_1 and Set_2 must be calculated from the solution vector X. A mapping function is performed to convert X to the corresponding binary vector V_b. Then, Set_1 and Set_2 are calculated from V_b according to (10). As mentioned before, the proposed work is based on predicting the background sub-spectrum B_RS_2 from either a normal or anomaly RS spectrum using a neural network model. Hence, the fitness function is used to evaluate the detection performance in terms of the prediction accuracy for a given Set_1 and Set_2. As can be seen from Fig. 7, the data pairs (fv, B_RS_2) calculated from the given spectra are divided into two groups for the respective training and testing of a neural network model, such that:

$$M_{tr} = \frac{2}{3} N_{tr}, \quad M_{ts} = \frac{1}{3} N_{tr}. \tag{14}$$

where M_{tr} and M_{ts} are the number of data used for training and testing the neural network model, respectively. The fitness value is calculated to evaluate the given solution X according to the prediction accuracy of the model as follows:

$$fitness\ value = \frac{1}{e_p}, \quad (15)$$

where e_p is the prediction error that is represented by the average Euclidian distance between the predicted and the actual B_RS_2 aver all the M_{ts} testing data. After performing the optimization process, the optimum solution is selected and the corresponding Set_1 and Set_2 are calculated.

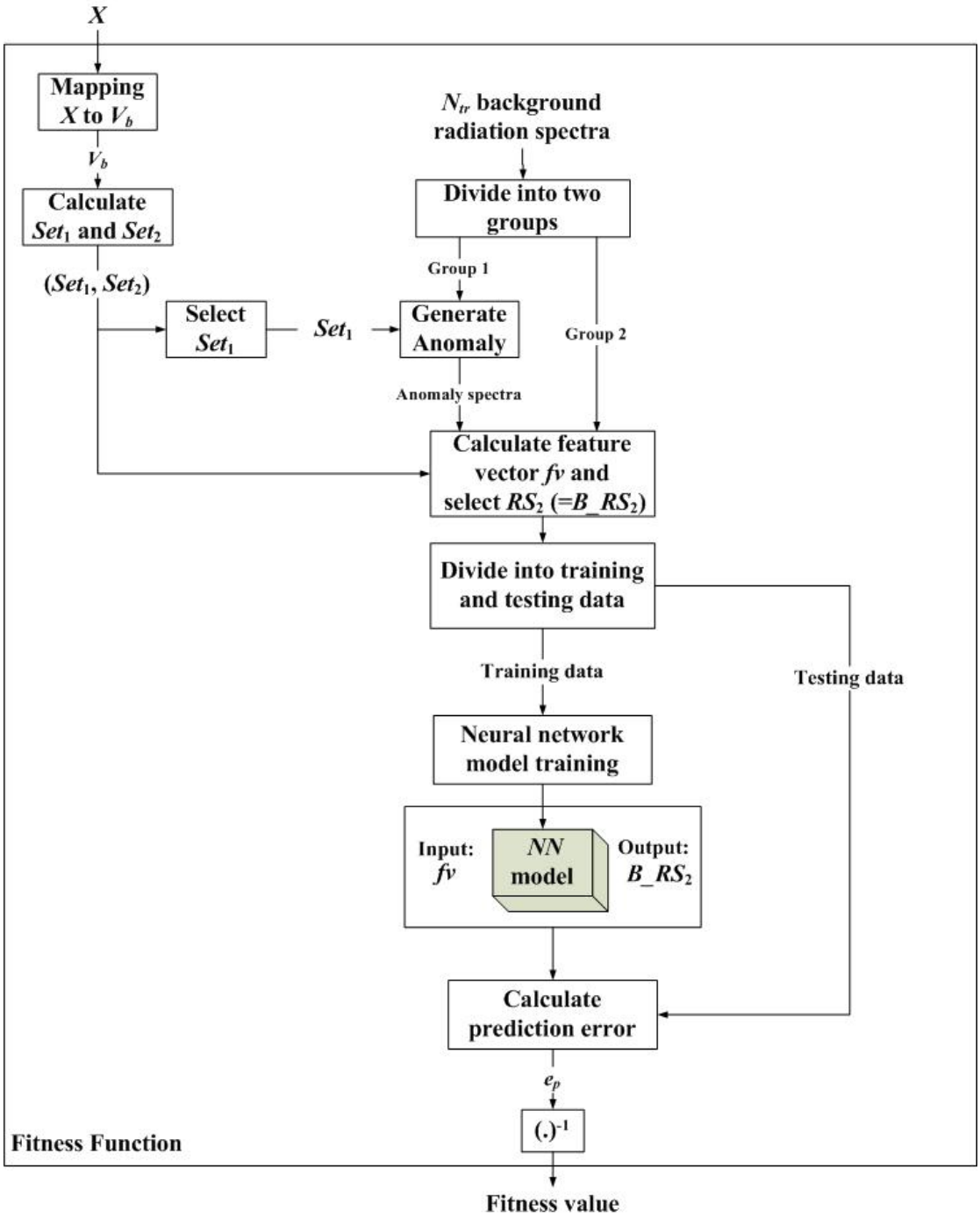

Fig. 7 The fitness function for evaluating the fitness value of a given solution X

4 Experimental results

In this section, the performance of the proposed work is evaluated and compared with other radiation anomaly detection methods. The performance is calculated using radiation spectra that are measured in the Savannah River National Laboratory at the Low Scatter Irradiator (LSI) facility [24]. The measurements were performed by 18 stationary radiation detectors deployed at different locations in a room of area 8 m × 8 m. Each detector measures the count rates at different energy bands, where 21 energy bands are selected to cover the energy range from 42 KeV to 2776 KeV. The normal (background radiation) data were collected by measuring the radiation spectra in the room without placing any radioactive sources as shown from Fig. 8. On the other hand, anomaly radiation spectra were measured from Cesium-137 and Cobalt-57 sources to provide three anomaly datasets referred to as: DS1, DS2, and DS3. Fig. 9 shows the layout for the radiation detectors and sources inside the room used for collecting the spectra in the three considered anomaly datasets. Note that the number of radiation spectra measured by a detector, in each of the anomaly datasets, is denoted by N_A. Table 1 presents the values of the parameters used for generating the datasets and implementing the proposed method. Note that the values of the parameters used for the implementation of the proposed method are selected experimentally.

Table 1 The values of the parameters used for generating the datasets and implementing the proposed work

Parameter			**Value**
Dataset:	Measurement parameters :	Area size:	8 m × 8 m
		Number of detectors:	18
		Type of detectors:	NaI (Sodium Iodide)
		Radiation source type:	Cesium-137 (^{137}Cs) and Cobalt-57 (^{57}Co)
		Source intensity *SI*:	7.6, 10, and 45 μCi
	Total number of background spectra N_D:		16197
	Total number of background spectra used for training N_{tr}:		12957
	Total number of background spectra used for performance evaluation N_{ts}:		3240
	Total number of anomaly spectra measured by each detector N_A:		840
	Number of spectral bins of the radiation spectrum N_b:		21
Neural Network (NN):	Number of hidden layers:		2
	Number of neurons per hidden layer:		6
	Activation function:		“relu”
Optimization:	Number of ants (population size):		10
	Number of iterations:		15
	Initial pheromone concentration:		0.2

	Evaporation rate:		0.5
	Solution space parameters:	Dimension D:	7
		Number of bits L:	3

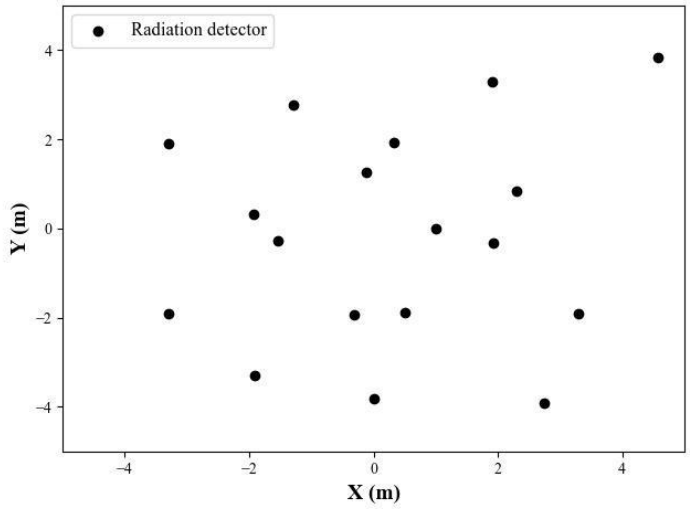

Fig. 8 Distributed radiation detectors for measuring background radiation inside a room of size 8 m × 8 m

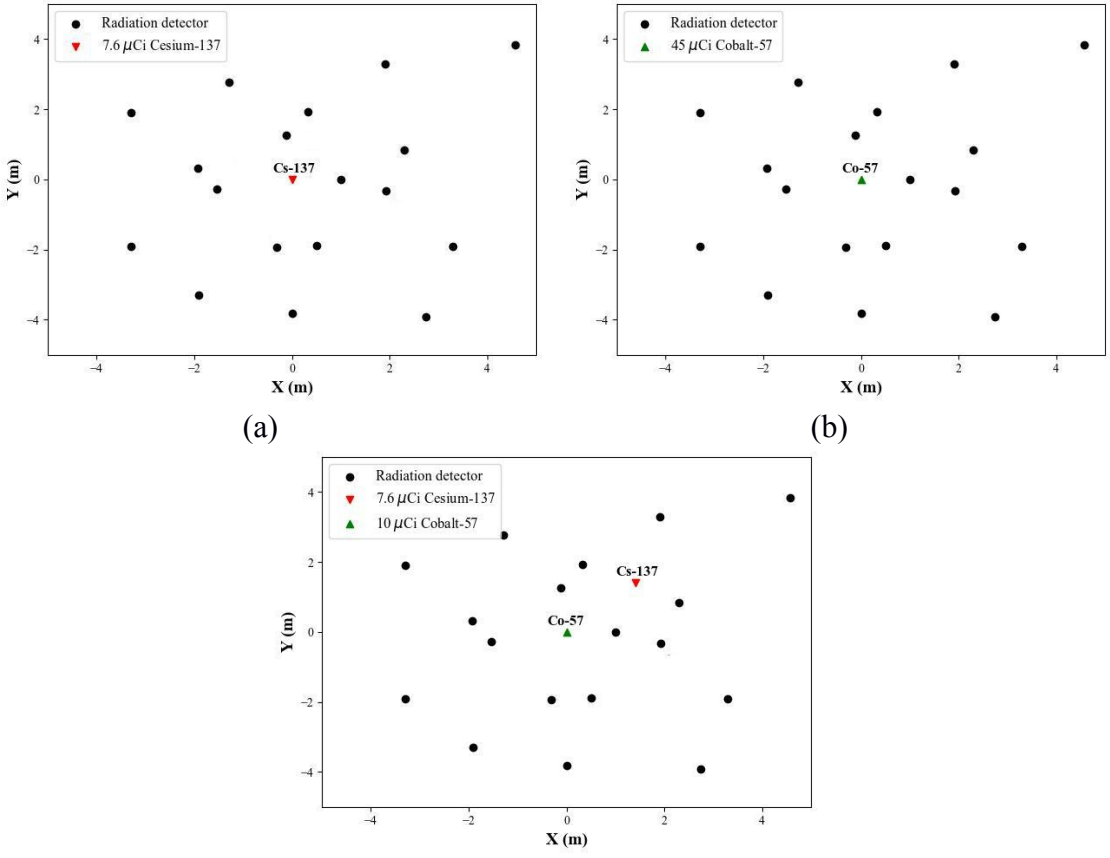

Fig. 9 Radiation detectors and a radiation source, inside a room of size 8 m × 8 m, for measuring the radiation spectra presented in datasets: (a) DS1, (b) DS2, and (c) DS3

It should be noted that the accuracy for detecting an anomalous source from the detector's readings depends on the source to background ratio (*SBR*) [11]. In this work, the source to background ratio is calculated for each detector as follows:

$$SBR_l = \varepsilon \frac{MGC_l - MGC_{BG}}{MGC_{BG}}, \quad (16)$$

where SBR_l is the value of the source to background ratio for the l^{th} detector. The constant ε presents a scaling factor, while MGC_{BG} and MGC_l are the mean gross count of the respective training background radiation spectra and the radiation spectra measured by the l^{th} detector. Note that the gross count is the summation of all the count values of the radiation spectrum. Accordingly, the values of MGC_{BG} and MGC_l can be calculated as follows:

$$MGC_{BG} = \frac{1}{N_{tr}} \sum_{i=1}^{N_{tr}} GC_{BG}[i], \quad MGC_l = \frac{1}{N_A} \sum_{j=1}^{N_A} GC_l[j], \quad (17)$$

where $GC_{BG}[i]$ and $GC_l[j]$ are the gross count values of the i^{th} and j^{th} spectrum corresponding of the respective background radiation and the radiation detected by the l^{th} detector. In Fig. 10, the *SBR* values for some of the detectors are presented, where the scaling factor ε is set to 10. As shown from Fig. 10, the *SBR* value decreases as the distance between the radiation source and the detector increases. It should be noted that the readings of the detectors that have very low *SBR* values represent only the background radiation. Consequently, only the spectra measured by the detectors with *SBR* values that exceed a defined threshold, denoted by thr_{SBR}, are considered as anomaly spectra. In other words, the *SBR* value and the threshold thr_{SBR} are used to represent the ground truth for the anomaly data. The calculation of thr_{SBR} is based on the observation of the radiation spectra at different *SBR* values. Fig. 11 shows the average background spectrum and four average spectra measured at four different *SBR* values, respectively. As can be observed, the detected radiation at *SBR* value of 0.49 can be considered as background radiation. The performance comparison is conducted at four different *SBR* thresholds thr_{SBR}, which are: 0.5, 0.7, 0.9, and 1.

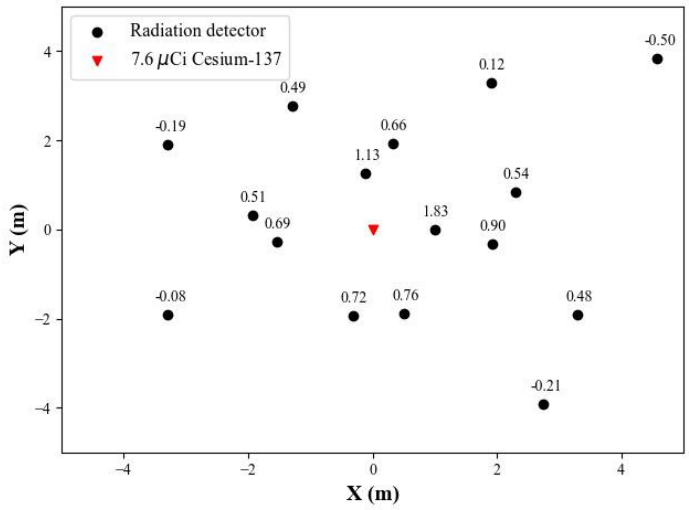

Fig. 10 The *SBR* value for the average radiation spectra measured by each detector for dataset DS1

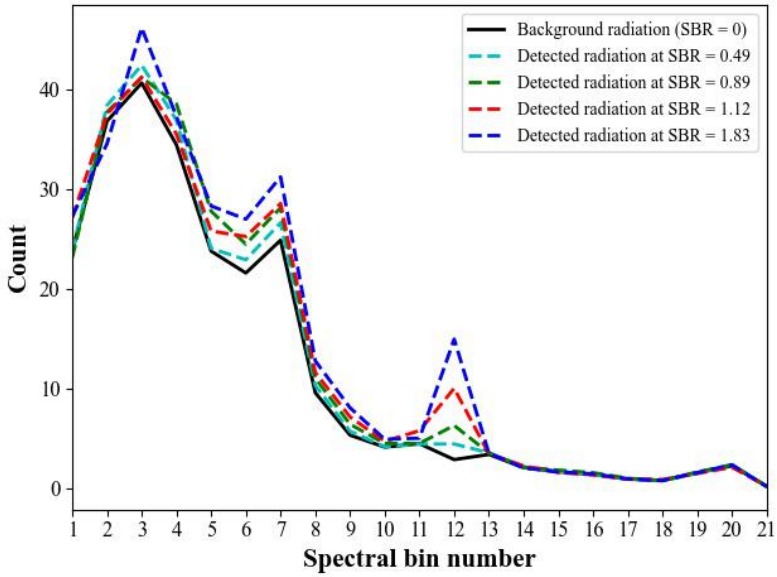

Fig. 11 Radiation spectra at different *SBR* values

Usually, the performance of the detection techniques is evaluated by the detection rate metric. However, in most of the anomaly detection problems, the amount of the available normal data is greater than that of the anomaly data as can be noted from Table 1. Thus, the detection rate will not provide an accurate performance metric due to the unbalanced dataset problem. In this work, accurate performance measurement is provided through the true positive rate (TPR), false positive rate (FPR), and the detection precision, which are defined as follows:

$$TPR = \frac{TP}{Total\ number\ of\ anomaly\ data},\quad (18)$$

$$FPR = \frac{FP}{Total\ number\ of\ normal\ data}, \quad (19)$$

$$Precision = \frac{TP}{TP + FP}, \quad (20)$$

where TP is the true positive value that represents the number of anomaly data that are correctly detected as anomaly. On the other hand, FP is the false positive value that indicates the number of normal data that are incorrectly detected as anomaly. The value of TP is evaluated using the anomaly spectra, while the value of FP is evaluated using the testing background radiation spectra. Accordingly, the total number of normal and anomaly data is equal to N_{ts} and N_A, respectively. To illustrate the detection performance adequately, the receiver operating characteristics (ROC) curve is presented, through which the TPR and FPR are calculated for different detection threshold thr_i. First, the anomaly score is calculated for all the training background radiation spectra. Note that, for the proposed method, the anomaly score is the Mahalanobis distance d_M as shown from Fig. 5. Then, the detection threshold value thr_i is calculated according to the following relation:

$$thr_i = \mu_d + k_i \cdot \sigma_d, \quad (21)$$

where μ_d and σ_d are the average and standard deviation of the anomaly score values corresponding to the background spectra, while k_i is the i^{th} value of a user-defined range of values. The threshold value, through which the best detection performance can be achieved, is selected as follows:

$$thr_d = \max_{thr_i} \left(TPR_i - FPR_i \right), \quad (22)$$

where TPR_i and FPR_i are the respective TPR and FPR calculated for the i^{th} threshold value thr_i. In this work, the performance comparison is carried out between the proposed method and three other anomaly detection techniques that are implemented according to their description in [4,14,25]. The methods are referred to as PCARAD (Principle Component Analysis-based Radiation Anomaly Detection) [25], SCRRAD (Spectral Comparison Ratio-based Radiation Anomaly Detection) [4], and ARAD (Autoencoder-based Radiation Anomaly Detection) [14]. Note that the performance is evaluated using the data measured by each detector, where the SBR value exceeds the threshold thr_{SBR}. Then, the final performance is presented by averaging the calculated performance corresponding to all the selected detectors.

In Fig. 12, 13, and 14, the ROC curves are shown for the proposed method, referred to as NNRAD (Neural Network-based Radiation Anomaly Detection), and the other methods in [4,14,25,26] for datasets DS1, DS2, and DS3, respectively. It is expected that the TPR and the FPR decrease as the detection threshold value thr_d increases and vice versa, which can be deduced from the ROC curve. At the same FPR values, methods that can provide higher TPR are considered better in terms of the detection capability. As can be seen from the results, the proposed method provides better detection compared to that of the other methods at all the considered values of the threshold thr_{SBR}. Furthermore, for $thr_{SBR} = 1$, the proposed method and the methods in [4,14] present almost the same performance. On the other hand, for smaller values of thr_{SBR}, the detection capability can be challenging, where different methods achieve different detection accuracy. The precision value is calculated using the detection threshold thr_d selected according to (22)**.** In Table 2, 3, 4, and 5, a comparison between the proposed method and the methods in [4,14,25] is presented in terms of the achieved precision calculated for $thr_{SBR} = 0.5$, 0.7, 0.9, and 1, respectively. Results show that the proposed work outperforms the other methods in terms of the detection precision even at low source to background radiation ratios (small values for thr_{SBR}).

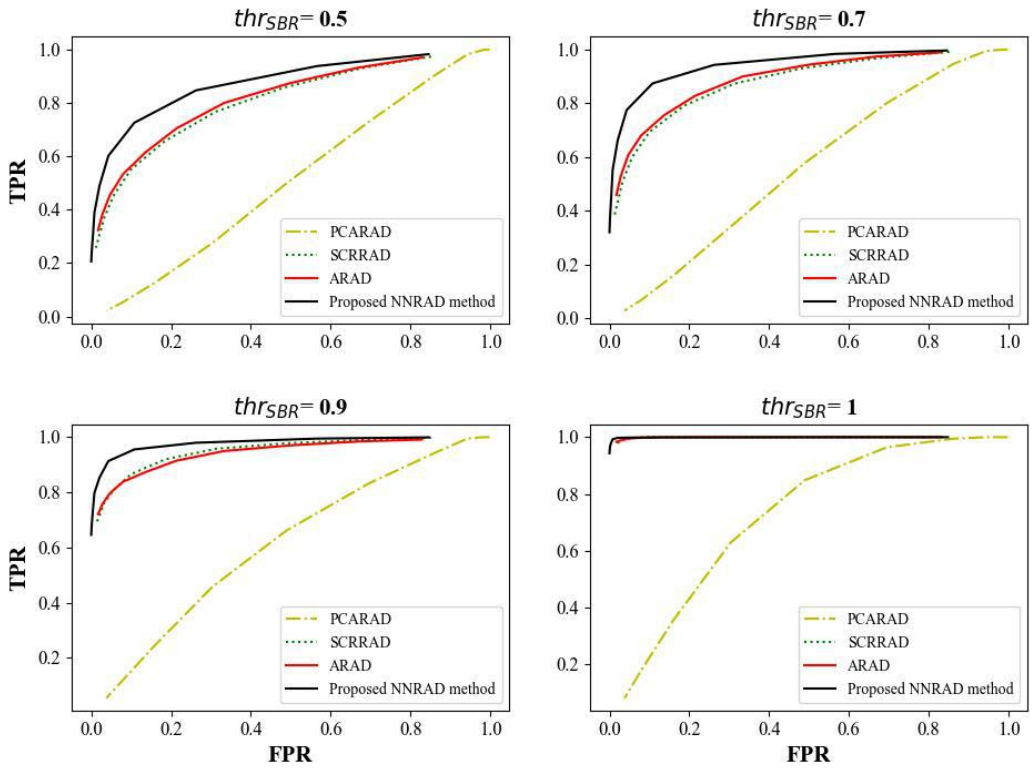

Fig. 12 ROC curves for the proposed NNRAD and the methods in [4,14,25] measured at different values for thr_{SBR} using dataset DS1

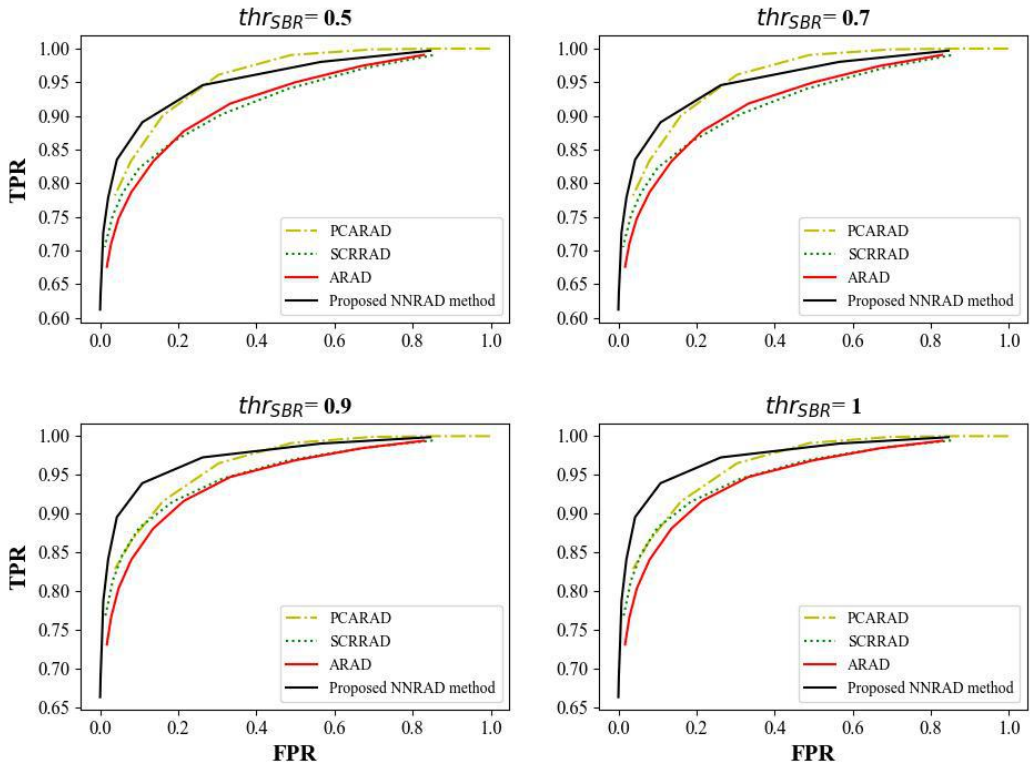

Fig. 13 ROC curves for the proposed NNRAD and the methods in [4,14,25] measured at different values for thr_{SBR} using dataset DS2

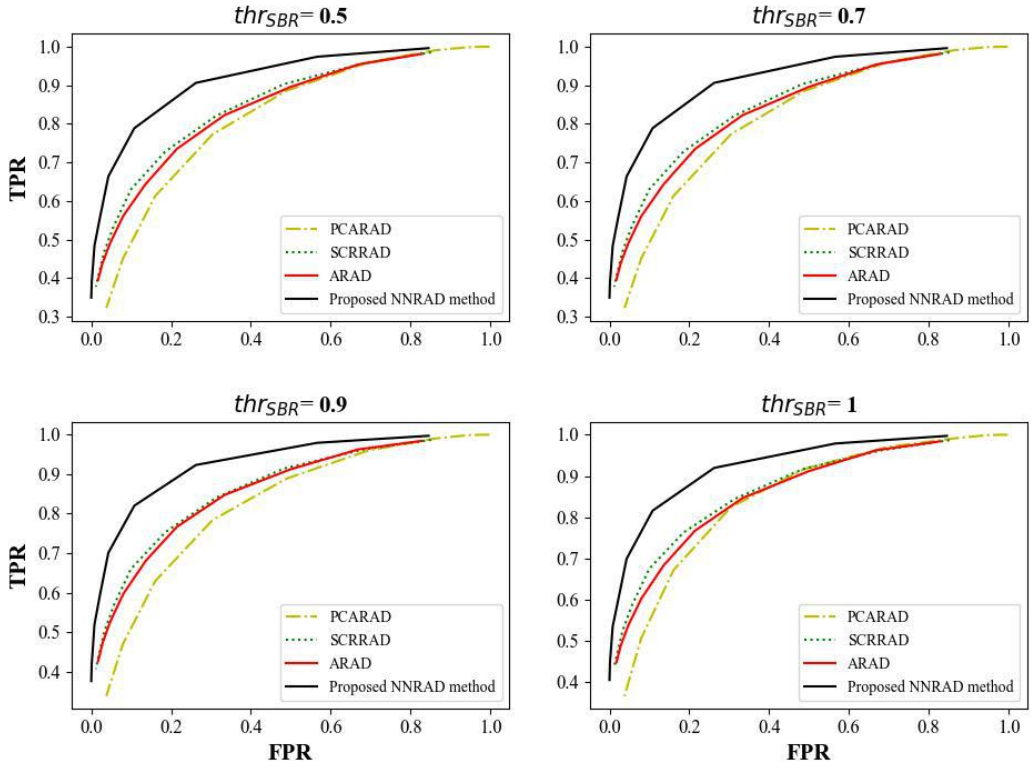

Fig. 14 ROC curves for the proposed NNRAD and the methods in [4,14,25] measured at different values for thr_{SBR} using dataset DS3

Table 2 Performance comparison between the proposed method and the methods in [4,14,25] in terms of the precision value measured for $thr_{SBR} = 0.5$

dataset	PCARAD [25]	SCRRAD [4]	ARAD [14]	Proposed NNRAD
DS1	0.212	0.457	0.299	0.513
DS2	0.741	0.742	0.716	0.743
DS3	0.351	0.452	0.420	0.503
Average:	**0.434**	**0.550**	**0.478**	**0.586**

Table 3 Performance comparison between the proposed method and the methods in [4,14,25] in terms of the precision value measured for $thr_{SBR} = 0.7$

dataset	PCARAD [25]	SCRRAD [4]	ARAD [14]	Proposed NNRAD
DS1	0.227	0.517	0.332	0.575
DS2	0.741	0.742	0.716	0.743
DS3	0.351	0.452	0.420	0.503
Average:	**0.439**	**0.570**	**0.489**	**0.607**

Table 4 Performance comparison between the proposed method and the methods in [4,14,25] in terms of the precision value measured for $thr_{SBR} = 0.9$

dataset	PCARAD [25]	SCRRAD [4]	ARAD [14]	Proposed NNRAD
DS1	0.249	0.682	0.444	0.759
DS2	0.804	0.787	0.745	0.777
DS3	0.353	0.461	0.433	0.516
Average:	**0.468**	**0.643**	**0.540**	**0.684**

Table 5 Performance comparison between the proposed method and the methods in [4,14,25] in terms of the precision value measured for $thr_{SBR} = 1$

dataset	PCARAD [25]	SCRRAD [4]	ARAD [14]	Proposed NNRAD
DS1	0.308	0.955	0.557	0.972
DS2	0.804	0.787	0.745	0.777
DS3	0.368	0.464	0.432	0.514
Average:	**0.493**	**0.735**	**0.578**	**0.754**

5 Conclusion

In this paper, we presented an anomaly detection method to distinguish between background and anomalous Gamma-ray radiation spectra. The method is based on dividing the radiation spectrum into two vectors, where each vector represents a sub-spectrum. The relation between the two sub-spectra was modeled through a neural network such that the background radiation data of one sub-spectrum can be predicted from the values of the other sub-spectrum. Accordingly, for a given radiation

spectrum, the error between the sub-spectrum and its predicted background values was used for measuring the anomaly score that was represented by the Mahalanobis distance. To consider anomaly data in the training process of the neural network model, a function was designed for simulating various anomaly spectra from the available normal spectra. Furthermore, the ACO was employed to optimize the selection of the radiation spectrum values assigned to each sub-spectrum, where optimum detection performance can be provided. A fitness function was designed, where the prediction error of the neural network model was computed to represent the fitness value to be optimized in the optimization process. The performance of the proposed work was evaluated and compared with other methods using real radiation data that had been measured via a network of radiation detectors. Experimental results showed that the detection capability of the proposed method is better than that of the other methods even at low source to background ratios.

Competing Interests: The authors declare that they have no known competing financial interests or personal relationships that could have appeared to influence the work reported in this paper.

Data availability statement: Our manuscript has no associated data.

References

1. IAEA: Incident and trafficking database (ITDB), https://www.iaea.org/resources/databases/itdb.
2. N. Trost, M. Iwatschenko, Method and device for detecting man-made radiation. ESM Eberline Instruments Strahlen-und Umwelmesstechnik GmbH, Germany, 1-14, (2002)
3. J. Ely, R. Kouzes, J. Schweppe et al., The use of energy windowing to discriminate SNM from NORM in radiation portal monitors. Nuclear Instruments and Methods in Physics Research Section A: Accelerators, Spectrometers, Detectors and Associated Equipment, **560**(2), 373-387, (2006). doi:10.1016/j.nima.2006.01.053
4. D. M. Pfund, R. C. Runkle, K. K. Anderson et al., Examination of count-starved gamma spectra using the method of spectral comparison ratios. IEEE Transactions on Nuclear Science, **54**(4), 1232-1238, (2007). doi:10.1109/TNS.2007.901202
5. K. K. Anderson, K. D. Jarman, M. L. Mann et al., Discriminating nuclear threats from benign sources in gamma-ray spectra using a spectral comparison ratio method. Journal of Radioanalytical and Nuclear Chemistry, **276**, 713-718, (2008). doi:10.1007/s10967-008-0622-x
6. R. C. Runkle, M. F. Tardiff, K. K. Anderson et al., Analysis of spectroscopic radiation portal monitor data using principal components analysis. IEEE Transactions on Nuclear Science, **53**(3), 1418-1423, (2006). doi:10.1109/TNS.2006.874883
7. M. F. Tardiff, R. C. Runkle, K. Anderson et al., Anomaly detection in gamma-ray vehicle spectra with principal components analysis and mahalanobis distances. (2006)
8. P. Tandon, P. Huggins, R. Maclachlan et al., Detection of radioactive sources in urban scenes using Bayesian Aggregation of data from mobile spectrometers. Information Systems, **57**, 195-206, (2016). doi:10.13140/RG.2.1.2050.7049
9. D. Boardman, M. Reinhard, A. Flynn, Principal component analysis of gamma-ray spectra for radiation portal monitors. IEEE Transactions on Nuclear Science, **59**(1), 154-160, (2012). doi:10.1109/TNS.2011.2179313
10. C. Zhang, G. Hu, F. Luo et al., Identification of SNM based on low-resolution gamma-ray characteristics and neural network. Nuclear Instruments and Methods in Physics Research Section A: Accelerators, Spectrometers, Detectors and Associated Equipment, **927**, 155-160, (2019). doi:10.1016/j.nima.2019.02.023
11. J. M. Ghawaly Jr, A Datacentric Algorithm for Gamma-ray radiation anomaly detection in unknown Background Environments. Doctoral Dissertation, University of Tennessee, 2020
12. M. Alamaniotis, A. Heifetz, Survey of Machine Learning Approaches in Radiation Data Analytics Pertained to Nuclear Security. Advances in Machine Learning/Deep Learning-based Technologies: Selected Papers in Honour of Professor Nikolaos G Bourbakis–Vol 2, 97-115, (2022). doi:10.1007/978-3-030-76794-5_6
13. J. Ghawaly, A. Young, D. Archer et al., A neuromorphic algorithm for radiation anomaly detection. In: Proceedings of the International Conference on Neuromorphic Systems 2022, 2022. pp 1-6. doi:10.1145/3546790.3546815
14. J. M. Ghawaly Jr, A. D. Nicholson, D. E. Archer et al., Characterization of the autoencoder radiation anomaly detection (ARAD) model. Engineering Applications of Artificial Intelligence, **111**, 104761, (2022). doi:10.1016/J.ENGAPPAI.2022.104761
15. A. Heifetz, L. Valdez, M. Alamaniotis, Detection of Anomalies in Environmental Gamma Radiation Background with Hopfield Artificial Neural Network. In: APS March Meeting Abstracts, 2022. p W31. 004. doi:10.2172/1827413

16. C. Sayre, E. C. Larson, G. DiLiegro et al., Radiation Anomaly Detection Using an Adversarial Autoencoder. In: 2023 57th Asilomar Conference on Signals, Systems, and Computers, 2023. IEEE, pp 1010-1014. doi:10.1109/IEEECONF59524.2023.10476882
17. A. Inamura, Asset Cueing Nuclear Radiation Anomaly Detection Using an Embedded Neural Network Resource. (2023)
18. S. Galib, P. Bhowmik, A. Avachat et al., A comparative study of machine learning methods for automated identification of radioisotopes using NaI gamma-ray spectra. Nuclear Engineering and Technology, **53**(12), 4072-4079, (2021). doi:10.1016/j.net.2021.06.020
19. A. Colorni, M. Dorigo, V. Maniezzo, Distributed optimization by ant colonies. In: Proceedings of the first European conference on artificial life, 1991. Paris, France, pp 134-142,
20. M. Dorigo, M. Birattari, T. Stutzle, Ant colony optimization. IEEE computational intelligence magazine, **1**(4), 28-39, (2006). doi: 10.1109/MCI.2006.329691
21. S. Pourtakdoust, H. Nobahari, An extension of ant colony to continuous optimization problems Proceedings of the ANTS 2004–Fourth International Workshop on Ant Colony Optimization and Swarm Intelligence, 2004. doi:10.1007/978-3-540-28646-2_27
22. K. Socha, M. Dorigo, Ant colony optimization for continuous domains. European journal of operational research, **185**(3), 1155-1173, (2008). doi:10.1109/ICNC.2012.6234538
23. L. Liu, Y. Dai, J. Gao, Ant colony optimization algorithm for continuous domains based on position distribution model of ant colony foraging. The Scientific World Journal, **2014**, (2014). doi:10.1155/2014/428539
24. N. S. Rao, S. Sen, M. Berry et al., Datasets for radiation network algorithm development and testing. In: IEEE Nuclear Science Symposium (NSS 2016), Strasbourg, France, 2016.
25. P. Tandon, Bayesian aggregation of evidence for detection and characterization of patterns in multiple noisy observations. AI Matters, **2**(3), 25-26, (2016). doi:10.1145/2911172.2911181
26. J. Lee, R. Cooper, T. Joshi et al., An Ensemble Approach to Computationally Efficient Radiological Anomaly Detection and Isotope Identification. IEEE Transactions on Nuclear Science, **69**(10), 2168-2178, (2022). doi:10.1109/TNS.2022.3198906